MDPI

Review

Current Research Status on Cold Sprayed Amorphous Alloy Coatings: A Review

Qiang Wang [1,2,*], Peng Han [1,2], Shuo Yin [3], Wen-Juan Niu [1,2], Le Zhai [1,2], Xu Li [1,2], Xuan Mao [1,2] and Yu Han [1]

[1] School of Metallurgical Engineering, Xi'an University of Architecture and Technology, Xi'an 710055, China; hangpeng90@163.com (P.H.); niuwenjuanmm@163.com (W.-J.N.); le.zhai@xauat.edu.cn (L.Z.); m18209264431@163.com (X.L.); xuan.mao@xauat.edu.cn (X.M.); yu.han@xauat.edu.cn (Y.H.)

[2] National and Local Joint Engineering Research Center for Functional Materials Processing, Xi'an University of Architecture and Technology, Xi'an 710055, China

[3] Department of Mechanical, Manufacturing & Biomedical Engineering, Trinity College Dublin, The University of Dublin, Dublin 2, Ireland; yins@tcd.ie

[*] Correspondence: qiang.wang@xauat.edu.cn

Abstract: Compared with traditional crystalline materials, amorphous alloys have excellent corrosion and wear resistance and high elastic modulus, due to their unique short-range ordered and long-range disordered atomic arrangement as well as absence of defects, such as grain boundaries and dislocations. Owing to the limitation of the bulk size of amorphous alloys as structural materials, the application as functional coatings can widely extend their use in various engineering fields. This review first briefly introduces the problems involved during high temperature preparation processes of amorphous coatings, including laser cladding and thermal spraying. Cold spray (CS) is characterized by a low-temperature solid-state deposition, and thus the oxidation and crystallization related with a high temperature environment can be avoided during the formation of coatings. Therefore, CS has unique advantages in the preparation of fully amorphous alloy coatings. The research status of Fe-, Al-, Ni-, and Zr-based amorphous alloy coatings and amorphous composite coatings are reviewed. The influence of CS process parameters, and powders and substrate conditions on the microstructure, hardness, as well as wear and corrosion resistance of amorphous coatings is analyzed. Meanwhile, the deposition mechanism of amorphous alloy coatings is discussed by simulation and experiment. Finally, the key issues involved in the preparation of amorphous alloy coatings via CS technology are summarized, and the future development is also being prospected.

1. Introduction

Amorphous alloys, also known as metallic glasses, have a unique short-range ordered atomic arrangement as opposed to long-range periodicity in crystalline materials [1,2]. Compared with traditional crystalline alloys, they have a series of unique properties, such as good corrosion and wear resistance, high hardness, sustainability [3,4], and elastic modulus. In addition, they have been widely used in marine ships, oil and gas pipeline transportation, nuclear power station, etc. [5]. Amorphous materials can be prepared by a variety of methods, either by a rapidly cooling liquid state to "freeze" them down, so that the material does not have time to crystallize, or by directly mixing atoms or molecules through ion beam mixing, physical vapor deposition, inter-diffusion solid phase reaction, mechanical alloying, severe plastic deformation, and laser preparation [6–8].

However, the wide application of amorphous alloys as structural materials faces great challenges. Mainly owing to the following reasons:

(1) The size of bulk amorphous alloys is limited. Due to the limited glass forming capacity and extremely high cooling rate (>10^5 K/s), the products of amorphous alloy

materials are mainly powders, wires or ribbons [9]. The size of the bulk amorphous alloy materials obtained by the casting process is in the centimeter level, which greatly restricts its application range [10].

(2)　The room temperature plasticity of amorphous alloy materials is poor. Unlike crystals which have slip bands, it is difficult to deform due to the special atomic structure of amorphous alloys. Deformation is confined to a highly concentrated shear zone [11]. When in a tensile stress state, once the shear band is generated and rapidly expanded, a brittle fracture occurs before the yield limit is reached, thus it has limitations when used as a load-bearing structural material [12,13].

In recent years, the application of amorphous alloys in the form of coatings has opened a new path to improve the surface properties in a harsh industrial environment, in particular of corrosion and wear resistance [14,15]. At present, the preparation technology of amorphous alloy coatings mainly includes laser treatment and thermal spraying technologies, such as plasma spraying, high velocity oxygen fuel, and high velocity arc spraying [16]. The laser cladding technology utilizes the characteristics of rapid heating and rapid cooling, the energy density is between 10^4–10^6 W/cm^2, and the cooling rate of the molten pool can reach 10^4–10^6 K/s [17]. The high energy density makes the cladding layer material and substrate material surface completely melt, resulting in an extremely thin molten pool depth. In addition, the cooling rate of the molten metal is much higher than the critical amorphous cooling rate of the alloy, thereby forming an amorphous coating on the surface layer [18]. Plasma spraying [19] uses a high-energy heat source to heat powder particles to a molten or semi-fused state in a short period of time. On the contrary, high velocity oxygen fuel spraying [20] and high-velocity arc spraying techniques [21] have the characteristics of higher spraying speed and lower spraying temperature. The particles which are sprayed at a certain speed to the surface of the substrate are spread and solidifies to form a layer, and the coatings are built up layer-by-layer [22,23]. However, the mentioned methods above are all based on high-temperature processes which involve the remelting of raw materials in the preparation of amorphous alloy coatings [24]. Therefore, the oxidation and crystallization phenomenon cannot be avoided and will result in the unstable composition and microstructural change of amorphous alloy, eventually affecting the service performance of coating materials [25]. In addition, the high temperature process will also have a negative impact on the substrate. Although the current process is constantly optimized to minimize this effect, surface oxidation and thermal damage still exist [26].

To overcome the aforementioned shortcomings during the preparation of amorphous coatings, cold spray (CS) technology, featured by low-temperature solid-state deposition, has demonstrated unique advantages in preparing temperature-sensitive amorphous coating materials. This article will introduce the principle of CS technology and present a comprehensive review of the current research status of CS manufactured amorphous alloy coatings, such as Fe-based, Al-based, Ni-based, Cu-based, and Zr-based coatings. The influential factors on the microstructure, hardness, wear resistance, and corrosion resistance of amorphous alloy coatings are mainly discussed. Additionally, the deposition mechanism of amorphous alloy coatings is explored.

2. Principle and Advantages of CS Technology

The CS technology originated in the 1980s. When scientists in the former Soviet Union conducted wind tunnel experiments, they found that when the velocity of particles exceeded a certain critical speed, the effect of particles on the target surface changed from erosion to deposition [27]. As shown in Figure 1, CS uses high-pressure gas (nitrogen, helium, or compressed air) to drive powder particles (1–50 μm) at a low temperature, which is far below the melting point of spraying powder materials, via a Laval nozzle to produce supersonic gas-solid two phases flow. The low-pressure and the high-pressure variant can be distinguished. In the low-pressure cold spray technology, nitrogen or air is pressurized to 0.5–1.5 MPa and the particle velocity can reach 800 m/s. The low-pressure cold spray system is portable and more economical. In the high-pressure cold spray technology, high-

pressure helium or nitrogen (3.0–5.0 MPa) is used as the carrier gas, and the particles can reach a higher velocity after passing through the Laval nozzle [28]. Compared with other thermal spraying technologies, as shown in Figure 2, the temperature of the CS process is much lower, which can effectively avoid oxidation, phase transition, thermal cracking, and other problems caused by the high temperature. Therefore, there are great advantages and potential in preparing temperature-sensitive amorphous coating materials [29,30]. During the CS process, the flying particles impact the surface of the substrate at a high speed (300–1200 m/s), and subsequently undergo severe plastic deformation to form a coating at a completely solid state. A wide range of metallic materials and metal-based composites can be deposited via CS [31–34]. Owing to the mechanism of solid consolidation, CS coatings generally have a near theoretical density as the bulk materials and beneficial compressive stresses.
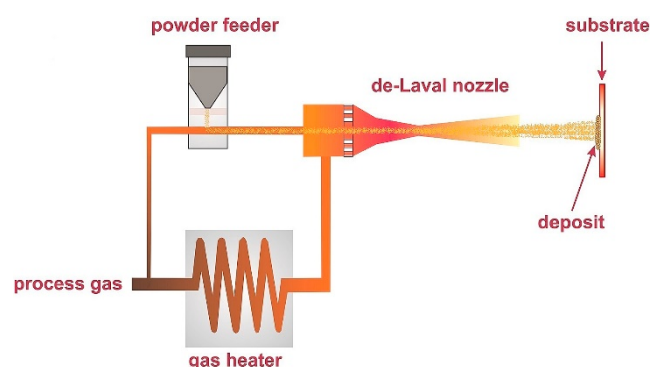

Figure 1. Principle of cold spray technology. Reprinted with permission from [31] Copyright 2021 Elsevier.
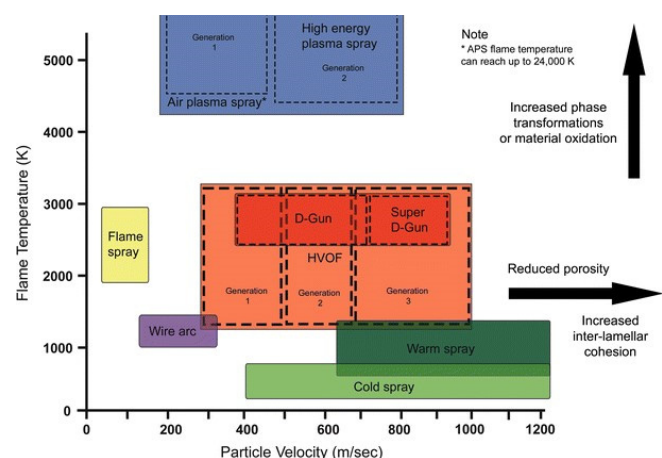

Figure 2. Temperature and velocity profiles of thermal and cold spray technologies. Reprinted with permission from [23] Copyright 2021 Springer.

3. Preparation and Properties of CS Amorphous Alloy Coatings

In the process of preparing amorphous alloy coatings using CS technology, the amorphous alloy powders are heated up to near the glass transition temperature (T_g) below the melting point to prompt a superplastic deformation ability, to form the coatings which retain the amorphous structure consistent with the original powder material. Table 1 lists the amorphous alloy coatings and basic process parameters prepared by CS, mainly including Fe-based [35–39], Al-based [40], Ni-based [41,42], Cu [43,44], and Zr-based [45] amorphous systems.

Table 1. Typical types and process parameters of cold spray (CS) amorphous alloy coatings.

Amorphous Alloy Coating Material	Substrate Material	Gas	Pressure/MPa	Temperature/°C	Ref
$Fe_{44}Co_6Cr_{15}Mo_{14}C_{15}B_6$	Al/Cu/Ti	N_2	4.0	900–950	[35]
$Fe_{73}Cr_2Si_{11}B_{11}C_3$	Carbon Steel	N_2	4.0–5.0	900–1000	[36,37]
Fe–Cr–Mo–W–C–Mn–Si–Zr–B	Al 6061	He	1	300	[38]
$Fe_{68.8}C_{7.0}Si_{3.5}B_{5.0}P_{9.6}Cr_{2.1}Mo_{2.0}Al_{2.0}$	Mild Steel	He	2.1–2.9	550	[39]
$Al_{88}Ni_6Y_{4.5}Co_1La_{0.5}$	Al 7075	N_2	3.0–4.0	300–400	[40]
$Ni_{57}Ti_{18}Zr_{20}Si_3Sn_2$	Mild Steel	He	3.0	600	[41,42]
$Cu_{50}Zr_{50}$	Stainless Steel	N_2	4.0	500–800	[43]
$Cu_{54}Ni_6Ti_{18}Zr_{22}$	Cu alloy	He	1.5–3	550	[44]
ZrCuAlNiTi	Cu	He	2.4	500	[45]

3.1. Fe-Based Amorphous Alloy Coatings

Fe-based amorphous alloys have the advantages of high hardness, excellent corrosion and wear resistance, good soft magnetic properties, and low cost. They are widely used in hydraulic machinery, motors, transformers, as well as electronics [46–48]. Ajdelsztajn et al. [38] synthesized Fe-based amorphous alloy coatings on a 6061aluminum alloy. Limited porosity was present in the coatings, and no micro-cracks can be observed between the deposited particles, despite the high deposition rate used (approximately 250 μm for a single layer). The micro-hardness reached 639 ± 16 Hv0.3, which was 12 times that of the substrate.

Choi et al. [49] reported that a gas atomized powder (~45 μm) with a composition of $Fe_{68.6}C_{7.1}Si_{3.3}B_{5.5}P_{8.7}Cr_{2.3}Al_{2.0}Mo_{2.5}$ (at.%) is deposited on a copper substrate using plasma spraying and cold spraying. The corrosion resistance of the amorphous alloy coating formed by the two methods in a 3.5% NaCl solution was also compared. Electrochemical measurements showed that both coatings exhibited relatively low corrosion currents ($<10^{-5}$ A/cm^2) and high pitting potentials (>1.0 V). In comparison, CS amorphous alloy coatings had a higher density and no oxidation, and their corrosion resistance was significantly better than that of plasma sprayed coatings. Yoon et al. [39] prepared the $Fe_{68.8}C_{7.0}Si_{3.5}B_{5.0}P_{9.6}Cr_{2.1}Mo_{2.0}Al_{2.0}$ (at.%) dense metallic glass coating on a low carbon steel substrate using helium as a carrier gas. As shown in Figure 3, the sprayed coating has a significantly higher hardness than the bearing samples and steel.
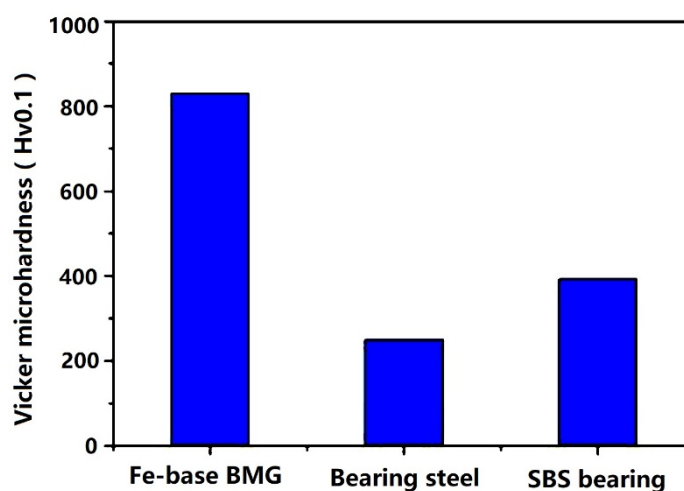

Figure 3. The average microhardness of the Fe-based BMG (bulk metallic glass) coatings, bearing steel, and SBS (steel-backed sintered) bearing. Reprinted with permission from [39] Copyright 2021 Elsevier.

3.2. Al-Based Amorphous Alloy Coatings

Al-based amorphous alloys have low density, high modulus, high specific strength, and excellent corrosion resistance. Their tensile strength is generally higher than 1000 MPa, and some can even reach 1500 MPa [50–52]. Compared with the ordered FCC structure in aluminum, the disordered atomic arrangement in the BMG structure makes it difficult to deform, while the slip surface in Al has a lower critical resolution shear stress (CRSS).

Lahiri et al. [53] synthesized an aluminum-based amorphous coating with $Al_{90.05}Y_{4.4}Ni_{4.3}Co_{0.9}Sc_{0.35}$ (at.%) powder through the CS technology, which was used to protect the surface of 6061 aluminum from corrosion and wear. Figure 4a showed the plot of wear volume vs. time for the substrate and coatings. Figure 4b showed the depth distribution of the wear track across the entire width. The maximum wear depth of the Al coating after 60 min was 30 μm, while the maximum wear depth of the 6061 Al coating was 135 μm. The amorphous coating had high hardness due to the glass properties, and the wear resistance was 600% higher than that of 6061 aluminum substrates. Figure 5 showed the typical potentiodynamic polarization curves of the coated sample and substrate in 0.01 and 0.1 N NaCl electrolytes. A Tafel fit was employed to analyze the polarization curves, and corrosion rates were obtained by extrapolating the Tafel slopes, as shown in Table 2. The substrate exhibited a higher passive current (9.8 and 28.7 μA) as compared with the coatings (2.0 and 6.3 μA). Under different NaCl concentrations, the corrosion resistance of the coating was five times that of the 6061 Al substrate.
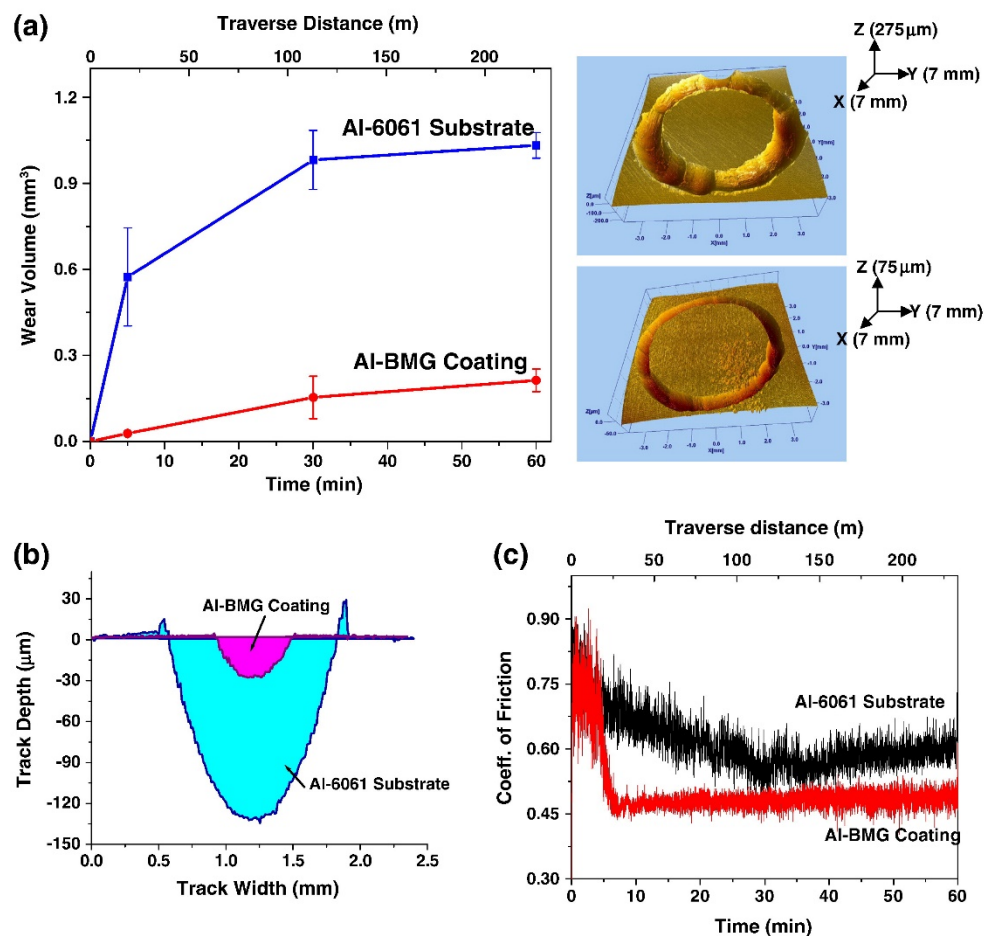

Figure 4. (**a**) Wear volume vs. time plot with respective SPM (Scanning Probe Microscope) images for tracks at 60 min, (**b**) profile of the track across the width after 60 min, (**c**) coefficient of friction vs. time plot for Al-BMG (Al-bulk metallic glass) coatings and Al-6061 substrate. Reprinted with permission from [53] Copyright 2021 Elsevier.
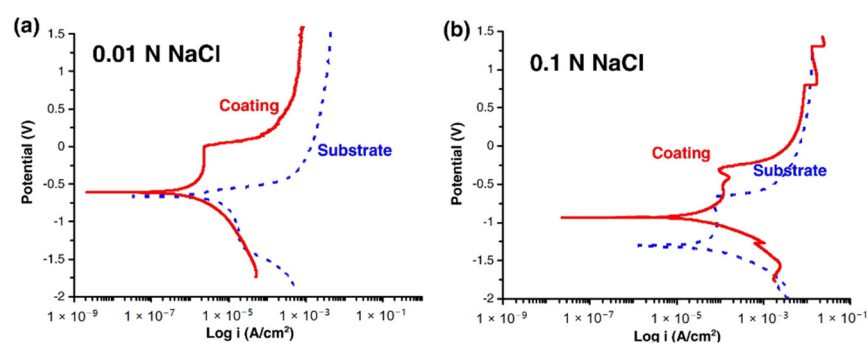
Figure 5. Potentiodynamic polarization curves for Al-BMG coatings and Al-6061 substrate in (**a**) 0.01 and (**b**) 0.1 N NaCl electrolyte. Reprinted with permission from [53] Copyright 2021 Elsevier.

Table 2. Corrosion behavior of Al-BMG coating and Al-6061 substrate at different concentrates of NaCl bath [53].

Sample/Bath	E_{corr}, V	I_{corr}, μA	Corrosion Rate, Mpy
Coating/0.01 NaCl	−0.705	1.960	3.012
Coating/0.1 NaCl	−0.869	6.260	9.593
Substrate/0.01 NaCl	−0.661	9.870	15.14
Substrate/0.1 NaCl	−1.310	28.7	44.0

Henao et al. [40] manufactured aluminum-based amorphous powders with a composition of $Al_{88}Ni_6Y_{4.5}Co_1La_{0.5}$ using a gas atomization method and sieved to obtain particles with a particle size between 20–40 μm. Figure 6a showed that with a load of 10 N, the wear resistance of the Al-based MG coatings was approximately twice that of the Al-7075-T6 substrate. Figure 6b showed the typical potentiodynamic polarization curves of Al-based MG coatings and Al7075-T6 alloy in a 0.6 M (3.5%) NaCl solution. Obviously, Al-based MG coatings spontaneously passivated from the corrosion potential at about −0.7 V up to at least −0.4 V. Rather, the Al-7075-T6 alloy showed a corrosion potential more negative than −0.8 V, while the pitting corrosion started at −0.7 V.
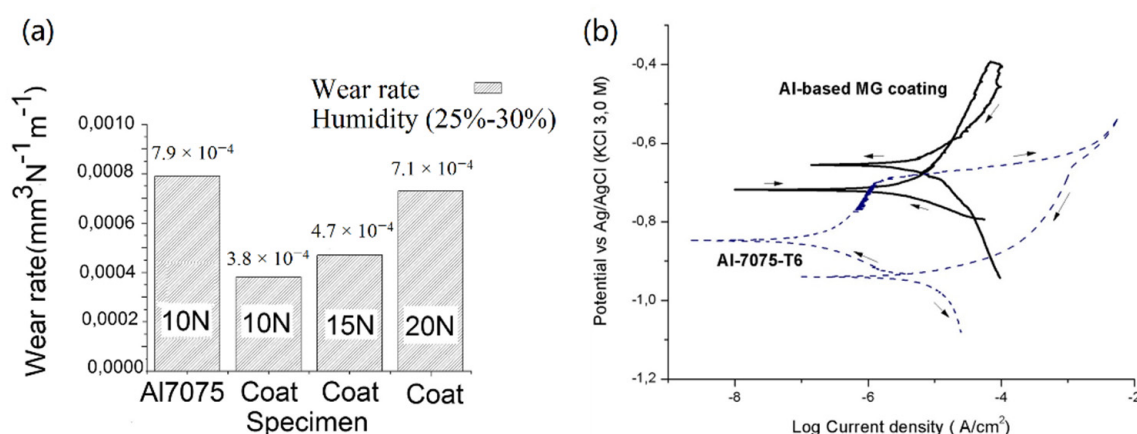
Figure 6. (**a**) Wear resistance of Al-based metallic glass coatings with different specimens (**b**) cyclic polarization curves for Al-based MG coatings and Al7075-T6 alloy. Reprinted with permission from [40] Copyright 2021 Elsevier.

Therefore, the wear resistance of Al-based MGs are better than that of crystalline Al-alloys, and show good coating resistance in a chloride environment. This shows that cold spray amorphous coatings can provide good surface protection.

3.3. Ni-Based Amorphous Alloy Coatings

Ni-based amorphous alloys have high thermal stability, high strength, and high corrosion resistance, and have often been used as corrosion-resistant materials. Although the development history of Ni-based bulk amorphous alloys is short, a relatively complete framework has been formed, mainly including three amorphous alloys such as Ni–Zr–Al, Ni–Ti–Zr, and Ni–Nb–Ti [54,55]. At present, the researchers have discovered that the bulk amorphous alloy system is based on the transition metal Ni–Fe and added metalloid element B or Si. In addition to having extremely high hardness, it also has high toughness, which has attracted special attention in the industrial field [56].

Yoon et al. [57] reported the deposition of $Ni_{57}Ti_{18}Zr_{20}Si_3Sn_2$ (wt.%) coatings onto a mild steel, by using the CS process. The results showed that increasing the speed and temperature of particles in flight can improve the mechanical properties and deposition efficiency. The kinetic energy and thermal energy of particles in flight had an important influence on the formation of the coatings. When helium was used as the processing gas, the particle impact speed was faster than that of nitrogen, and the deposition of the bulk amorphous feedstock resulted in a very dense coating microstructure. The bond strength and hardness increased with the increase of the particle temperature. Choi et al. [41] conducted a comparative study of $Ni_{57}Ti_{18}Zr_{20}Si_3Sn_2$ (wt.%) amorphous coatings prepared by the CS and thermal spraying processes, including vacuum plasma spraying and high velocity oxy-fuel (HVOF) spraying. This study had proved that the phase evolutions of the as-sprayed amorphous coatings were largely dependent on the impacting particle energy and the oxidization of original amorphous powders in the processing environment. Figure 7 showed the cross-section backscattered electron images and XRD test results of the amorphous coatings. The coating material prepared by the CS technology maintained the amorphous structure characteristics as completely consistent with the original powder material. However, the use of HVOF and VPS technology resulted in the oxidation and crystallization. Wang et al. [58] studied the effect of crystallization degree on the corrosion properties of amorphous alloy coatings. Partial amorphous $Ni_{59}Zr_{20}Ti_{16}Si_2Sn_3$ (wt.%) and $Ni_{53}Nb_{20}Ti_{10}Zr_8Co_6Cu_3$ (wt.%) alloy coatings were prepared by high velocity air fuel (HVAF) thermal spraying, whereas fully amorphous $Ni_{53}Nb_{20}Ti_{10}Zr_8Co_6Cu_3$ (wt.%) alloy coatings were obtained by the CS technique. It was shown that the partial amorphous $Ni_{53}Nb_{20}Ti_{10}Zr_8Co_6Cu_3$ alloy coatings, with an amorphous phase content of 77%, exhibited a lower corrosion resistance than that of the fully amorphous metallic coatings in a 1 M HCl aqueous solution.
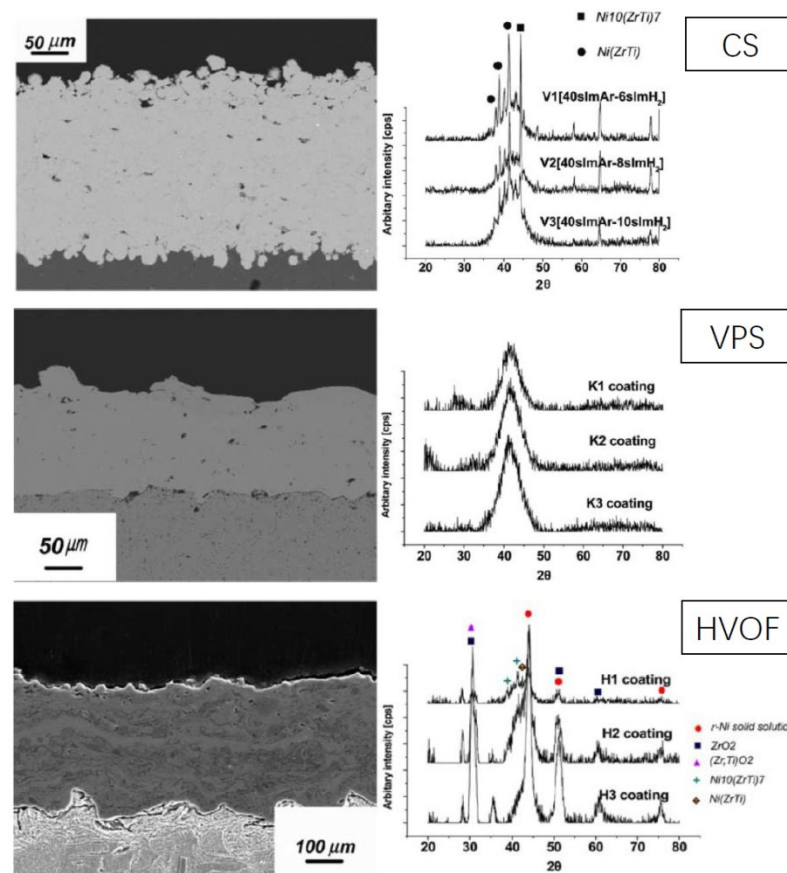
Figure 7. Cross-sectional backscatter electron micrographs (left) and XRD phase analysis results of Ni-based amorphous coatings prepared by cold spray and thermal spray techniques. Reprinted with permission from [41] Copyright 2021 Elsevier.

3.4. Cu-Based Amorphous Alloy Coatings

Cu-based bulk amorphous alloys have many excellent properties, such as high strength, high hardness, and strong corrosion resistance. In addition, they have broad application prospects in the industry, including aerospace, electronics, medical, and sports equipment fields [59]. In the present research, Cu-based amorphous alloy coatings are mainly focused on Cu–Ti, Cu–Zr binary alloy systems, and the preparation of highly corrosion resistant Cu-based amorphous alloy coatings has attracted great interest for medical applications in recent years [60,61].

Lee et al. [62] used CS as a new fabrication process to produce Cu-based amorphous ($Cu_{54}Zr_{22}Ti_{18}Ni_6$) coatings. The macroscopic properties and microstructures of the amorphous coatings were studied and compared with those of the cold spray pure Cu coatings. For Cu-based amorphous coating layers and pure Cu, the measured hardness was 412.8 and 145.1 Hv, respectively. Figure 8 showed the test results of the wear performance of the two coatings. The figure showed that the wear resistance of the Cu-based amorphous coatings was more than three times that of the pure Cu coating. This was consistent with the previous hardness test results. Sherif El-Eskandrany et al. [63] obtained a metastable phase of metallic glassy $Cu_{50}Ti_{20}Ni_{30}$ alloy powders through low-energy ball milling. Different from using the gas atomized amorphous alloy powders, the powder had an average particle size of 1.7 μm in diameter with spherical-like morphology. The $Cu_{50}Ti_{20}Ni_{30}$ coatings with a thickness of about 10 μm were deposited onto SUS 304 steel substrate. The nanohardness and Young's modulus obtained from 88 points were plotted in Figure 9a,b. The metallic glassy $Cu_{50}Ti_{20}Ni_{30}$ coating material had a very high microhardness value, ranging between 2.97 and 3.20 GPa, as shown in Figure 9a. In addition, in Figure 9b, the value of Young's modulus measured from 88 selected points showed a variation in the

range between 97 and 111 GPa depending on the XY coordination of each examined point. As for the sliding wear behavior of metallic glass coatings, from 150 s to the end of the sliding time, the COF of SUS304 reached 0.83 without any significant changes (Figure 10a). However, in the sliding time of 50 to 500 s, the COF value of the $Cu_{50}Ti_{20}Ni_{30}$ coating sample reached 0.48, as shown in Figure 10b.
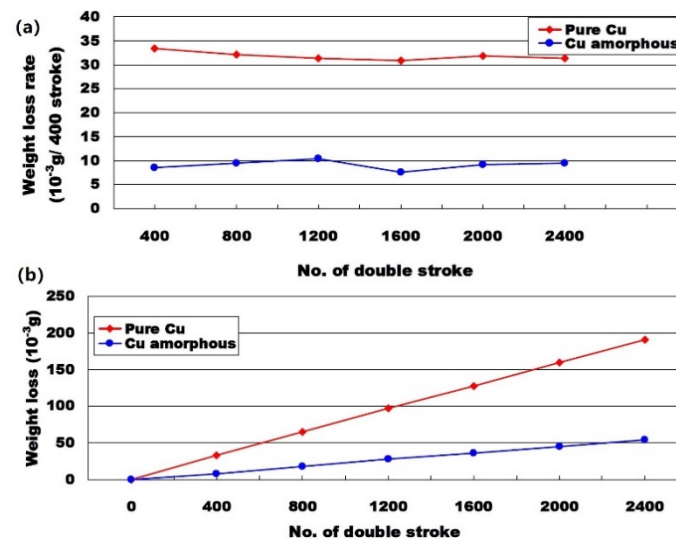
Figure 8. Wear performance of the pure Cu and Cu-based amorphous coatings; (**a**) weight loss rate and (**b**) weight loss [62].
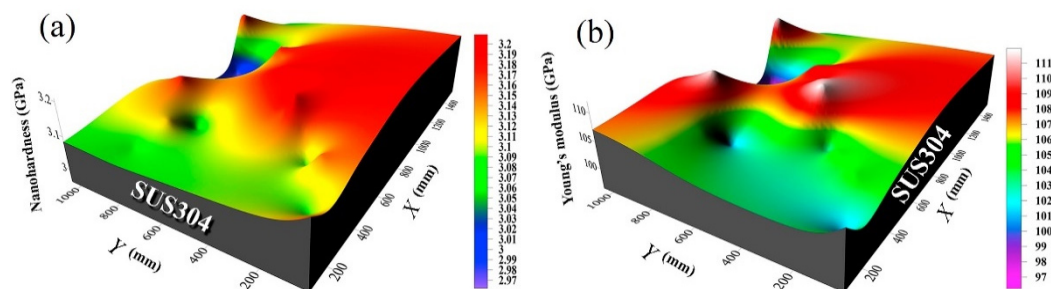
Figure 9. (**a**) The nanohardness and (**b**) Young's modulus results are shown in isometric projections. Reprinted with permission from [63] Copyright 2021 Elsevier.

Figure 10. Dynamic COF (coefficient of friction) curves of (**a**) uncoated SUS304 substrate, and (**b**) cold spray metallic glassy $Cu_{50}Ti_{20}Ni_{30}$ powders coated SUS304. Reprinted with permission from [63] Copyright 2021 Elsevier.

3.5. Zr-Based Amorphous Alloy Coatings

Zr-based amorphous alloys have high tensile strength, high elastic energy, high impact fracture performance, high corrosion resistance, good biocompatibility, and high electroca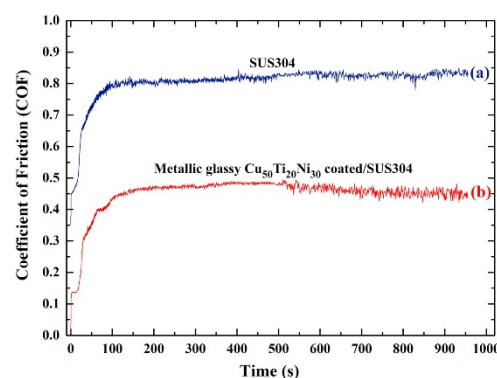talytic activity. It has huge application prospects in sports equipment, electronics, and medical fields [64]. Zr-based amorphous alloys have a strong glass-forming ability (GFA) and a wide supercooled liquid region. Zr–Cu–Al–Ni and Zr–Cu–Al–Ni–Ti are the two most commonly used alloys at present [65].

Kang et al. [45] added 5 wt.% of $Zr_{62}Cu_{26}Al_4Ni_5Ti_3$ amorphous powder as reinforcing particles to copper powder to prepare composite coatings by the CS process, and discussed the microstructure and mechanical properties. Figure 11a illustrated the typical composite microstructure observed by SEM back-scattered images, where the bright particles corresponded to the amorphous alloy reinforcements. Meanwhile, a significant plastic deformation was observed for Cu particles in Figure 11b. The porosity of deposits was measured lower than 0.1%, which was even lower than that of pure copper deposits (0.3%). This reduction in the porosity level was attributed to the result of a significant hammering effect of the amorphous alloy particles. The addition of amorphous alloy particles had also greatly improved the mechanical properties of composite materials, i.e., the tensile strength reached over 366 MPa at room temperature, and the microhardness was higher than 125 HV, and the elongation also increased from 3.0% to 6.6%. A mixed wear behavior of adhesive, abrasive, and corrosive was observed from the tribology test. The wear rate of CS composite coatings had been greatly reduced to 0.62×10^{-5} mm^3/(N·m), compared with 3.56×10^{-5} mm^3/(N·m) of pure copper coatings.

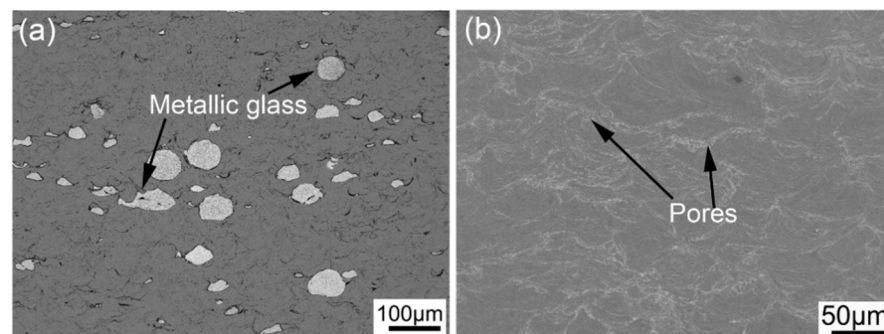**Figure 11.** Cross-sectional microstructure of (**a**) composite deposits and (**b**) Cu deposits after chemical etching. Reprinted with permission from [45] Copyright 2021 Elsevier.

4. Deposition Mechanism of CS Amorphous Alloy Coatings

In the CS process, the deposition starts from the initial collision of high-velocity particles with the substrate. When the particle velocity (V_p) is below the critical velocity (V_c), the particles will rebound, when V_p is between V_c and erosion velocity (V_e), the particles will bond with the substrate to form coatings. As V_p exceeds V_e, erosion occurs [29,33,66]. In fact, the particle impact occurs within an extremely short time of tens of nano-seconds, and the strain and strain-rate at the particle/substrate interface can reach up to 10 and $10^8 \sim 10^9$ s^{-1}, respectively, and the temperature rises rapidly at the interface at a heating rate of 10^9 K/s [66]. Therefore, the particle deformation is under an extremely complex condition. On the other hand, the deformation of particles under a high-velocity impact is concentrated in the surface region. Upon impact, one part of the kinetic energy of flying particles is transformed into strain energy and the other is converted into thermal energy. The localized temperature may reach the vicinity of the melting point of the particles, resulting in the deformation under a high temperature and high strain rate. Compared with the surface region, there is less deformation inside the particles, and the temperature rise is not obvious, which belongs to a low temperature and low strain rate deformation zone.

List et al. [43] studied the deformation behavior of the $Cu_{50}Zr_{50}$ amorphous alloy single particle impact during CS by a systematic variation of the spray parameters, and

determined the critical speed of coating formation through experiments. A particular challenge in the CS deposition of amorphous alloys is that the deformation upon impact highly depends on the particle temperature rather than the particle velocity in crystalline materials, which can be explained with respect to a universal time-temperature-transformation (TTT) diagram, as shown in Figure 12. In region ① when particle temperatures are below the glass transition temperature (T_g), the amorphous particles exhibit mainly brittle behavior, i.e., no plastic deformation upon impact, resulting in a crater on the surface with poor bonding to the substrate and within the coatings. In contrast, at particle impact temperatures far above T_g, but below conditions for crystallization, in the state of an undercooled liquid, region ②, a liquid-like behavior is expected. This is mainly through viscous flow leading to highly deformed flat particles, but at the cost of increased crystallization risk. At particle temperatures slightly below the T_g, region ③, the formation of local shear bands caused by the high strain rate deformation during impact is related to the local heat generation. The respective temperature rise and deformation can further facilitate bonding.
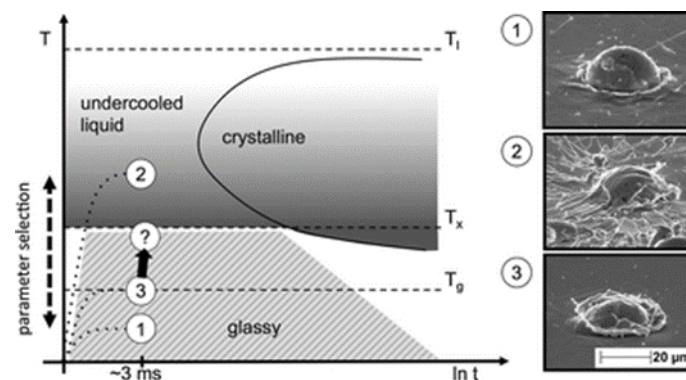

Figure 12. Amorphous metals schematic time temperature transformation (TTT) diagram. Reprinted with permission from [43] Copyright 2021 Springer.

Figure 13 shows examples of single particle impact morphologies, as classified into the four different impact categories. The different classes are provided in the following: (a) No bonding, particles leave empty craters in the substrate, (b) weak bonding, mainly undeformed particles stick to the substrate or are partially detached, (c) good bonding, particles stick completely to the substrate and show localized deformation at the interface, and (d) viscous flow, particles mostly behave as an undercooled liquid. It is assumed that due to the lack of sufficient deformation, classes (a) and (b) could not contribute to the formation of the coating. Particles exhibiting (c) shear instability or (d) sticky behavior are expected to contribute to the formation of the coatings, which corresponds to regions ② and ③, respectively in the TTT diagram.

For crystalline materials, Assadi et al. [67] proposed that coatings can be produced without significant heating of the sprayed powder. In this process, the bond of particles was due solely to their kinetic energy upon impact. It used a numerical model of deformation during the particle impact to provide a hypothesis for particle bonding in cold gas spraying. The analysis showed that the bonding was caused by the adiabatic shear instability of the surface due to particles exceeding the critical velocity. Copper based particles were taken as the research object. First, in the process of high-speed particle collision with the substrate, a local slow-diffusion heating process occurred near the particle/substrate interface in a very short period of time. In subsequent analyses, Figure 14 showed the development of plastic strain, temperature, and flow stress in a so-called critical element at the particle surface which undergoes the highest amount of deformation within the particle. As the initial particle velocity increased from 550 to 580 m/s, the trends of these variables change over time, indicating shear instability. This phenomenon can be explained by the change of deformation mechanism from plastic to viscous flow. Near thermal softening conditions, the resistance of the material to shear flow was usually low. This means that by

approaching the melting temperature, the material lost its shear strength and will deform excessively when any amount of shear stress was applied.
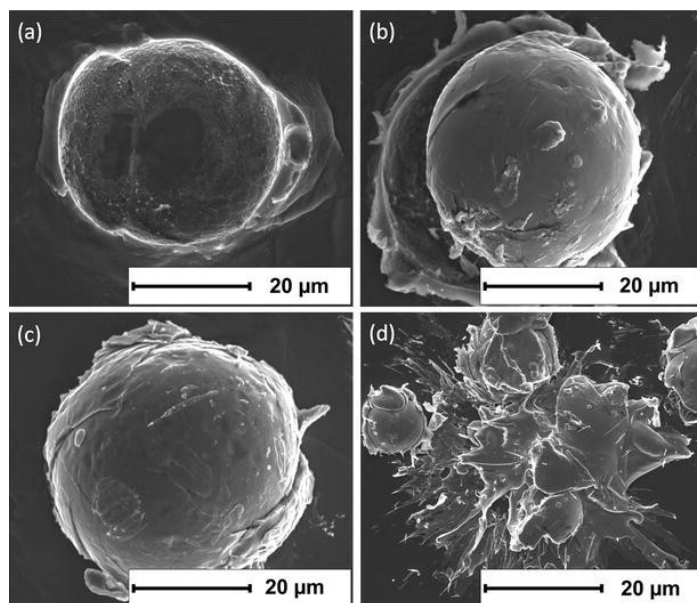
Figure 13. Different classes of particle deformation. (**a**) No bonding, (**b**) weak bonding, (**c**) good bonding, and (**d**) viscous flow. Reprinted with permission from [43] Copyright 2021 Springer.
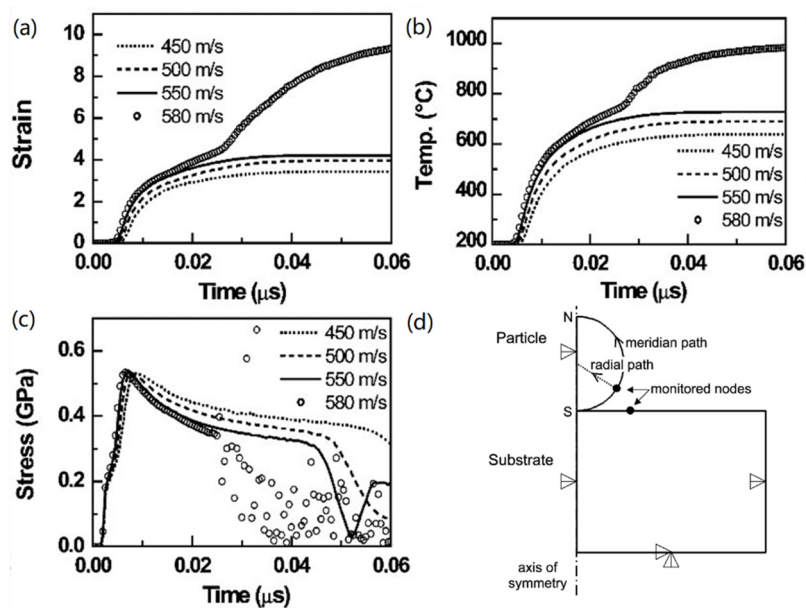
Figure 14. Calculated temporal development of (**a**) plastic strain (**b**) temperature, and (**c**) flow stress at the node (as indicated in (**d**)) of a sprayed particle for various impact velocities. Reprinted with permission from [67] Copyright 2021 Elsevier.

According to the thermal properties of the amorphous alloy, when it is heated above the glass transition temperature (T_g), the amorphous alloy will become a low-viscosity supercooled liquid [68]. Amorphous alloys are considered viscoplastic materials, and their plasticity depends on the liquid's Newtonian viscosity, following the Vogel-Fulcher-Tamman (VFT) equation. Under the extreme conditions of high strain rate and effective thermal softening, the effective thermal softening of impact particles can be regarded as

Newtonian flow. Amorphous plasticity has two different deformation modes: Homogeneous flow (non-localized deformation uniformly distributed) and inhomogeneous flow (localized deformation by means of shear band formation). The type of flow is dependent only on the strain rate and temperature [69]. Therefore, the previous research on the use of CS to produce amorphous alloy coatings is conducted under the concept of thermal softening between the glass transition temperature (T_g) and the crystallization temperature (T_x). However, preheated particles higher than T_g are not the only requirement for the deposition of metallic glasses, since their mechanical response also depends on the strain rate upon impact. At high temperatures and high strain rates, inhomogeneous flow can occur and lead to poor deposition of amorphous alloy particles. In fact, not only the shear band is promoted at high strain rates and low temperatures, but if the strain rate is high enough, shear bands are also formed at temperatures of about T_g and above.

　　Assadi's research was focused on crystal particles. However, the simulation does not include considerations of the properties and deformation mechanisms of MGs in the supercooled liquid region. Therefore, for amorphous, there is still a lot to be improved. On the basis of the former, Henao et al. [70] adopted the constitutive equation of a free volume model to simulate the homogenous flow deformation in Newtonian and non-Newtonian systems. The calculated results were compared with the experimental data of the metallic glass coating formed by cold spraying. Both experiments and simulations had found the critical value of Reynolds number (Re), indicating that it was a useful parameter to control the activation of bonding of metallic glass particles and viscoplastic deformation. The experiment simulated the Von Mises yield criterion (VM) stress of different Re, as shown in Figure 15. With the increase of Re, the VM equivalent stress distribution within the MG particle was gradually homogeneous. This can be interpreted as the MG particle flows easily due to the enhanced softening. Inhomogeneous flow mainly occurs below the critical Re. When Re exceeds the critical value, the viscoplastic flow increases, and the inhomogeneous flow (accompanied by the formation of shear bands) was transformed into the homogeneous flow. It showed that the MG particle was deposited and bonded due to the homogeneous deformation experienced during impact and the high temperatures achieved at the particle/substrate interface (allowing for the formation of a metallurgical bond). It also proved that the deposition of metallic glass particles was controlled by the coordinated movement of the liquid. Unlike polycrystalline metals, there was no simple shear instability effect at the particle-substrate interface.
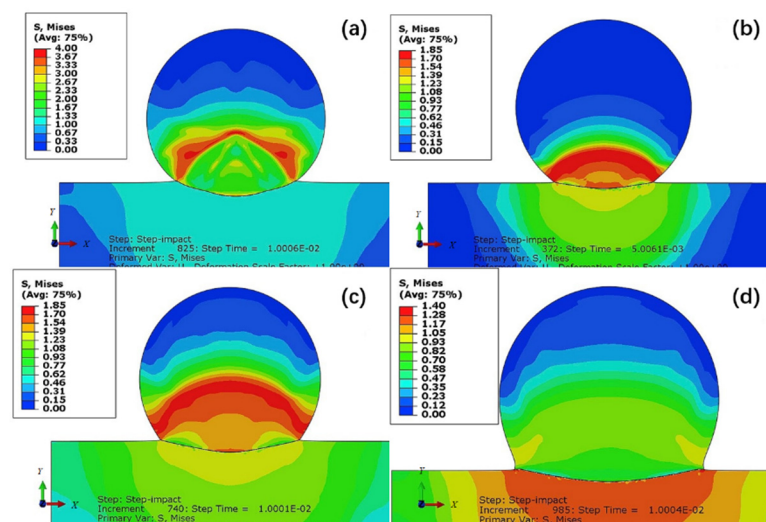

Figure 15. Simulation of Von Mises (VM) equivalent stress contours at 10 ns with different Re. (**a**) Re = 1.77×10^{-9}, (**b**) Re = 3.35×10^{-5}, (**c**) Re = 4.45×10^{-5}, (**d**) Re = 0.229. Reprinted with permission from [70] Copyright 2021 Elsevier.

The deformation mechanism of MG particles deposited by CS has not been fully understood. In the simulation process, the constitutive equation of the free-volume model is used to approximately describe the deposition principle of MG particles and allow the calculation of deposition windows of different MG particles, but this model is not applicable to the inhomogeneous flow. Therefore, the deformation mechanism of MG particles deposited by CS is still worth further exploration. Due to the extremely short impact time of particles, the focus of future research on the deposition mechanism of MG particles may be to study inhomogeneous flow models to simulate the impact process of amorphous particles.

5. Influencing Factors on the Microstructure and Properties of Amorphous Alloy Coatings

The performance of amorphous alloy coatings mainly depends on the integrity of the amorphous structure, which is affected by key factors, including the characteristic of original amorphous alloy powder, spraying parameters, and thermo-mechanical properties of the substrate materials.

5.1. Powder Characteristics

At present, amorphous alloy powder material systems mainly include Fe-based, Al-based, Ni-based, Cu-based, Zr-based, etc. Such materials have a good glass forming ability, and the particles formed have well composition uniformity. The size of the powder and the composition of the alloy strongly influence the deposition and deformation behavior of the particles, and therefore the deposition efficiency (DE) during spraying.

Early research clearly illustrated the relationship between critical velocity, impact velocity, and particle size by Schmidt et al. [71]. As shown in Figure 16, small particles can be accelerated to a relatively high speed, but were decelerated in the bow shock in front of the substrate. The critical velocity decreased with the increasing particle size and then stabilized. To obtain the optimal size range, the selected area where the impact velocity was higher than the critical velocity and the particles are deposited under relatively appropriate impact conditions. Reasonably selecting a narrow particle size range of amorphous alloy particles is conducive to improve the deposition efficiency of the amorphous alloy coatings.
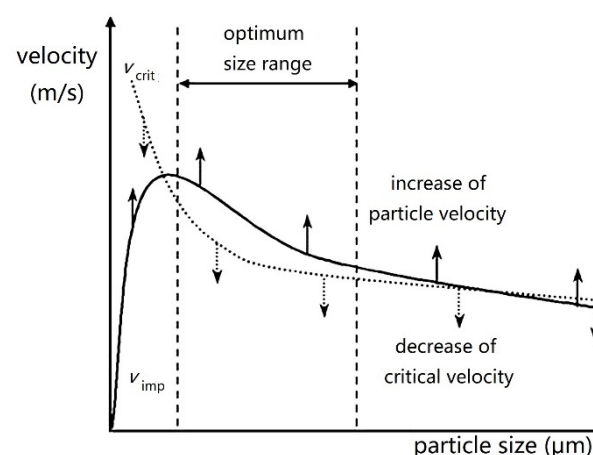
Figure 16. Optimization of particles size range according to the critical and impact velocities. Reprinted with permission from [71] Copyright 2021 Springer.

Song et al. [72] investigated the influence of non-spherical particles on the impact velocity for different working parameters of the gas streams by using computational fluid dynamics modeling. The shape factor (φ) was used to quantify the degree of sphericity of the non-spherical particle [73].

$$\varphi = \frac{A_{sp}}{A} \tag{1}$$

where A_{sp} is the surface area of the sphere of the same volume as the non-spherical particle and A is the actual surface area of the particle. The results showed that due to the larger specific surface area, the velocity of particles with a smaller shape factor can more easily reach the velocity of the high-pressure carrier gas. Within a certain range, the particle deposition efficiency increases with the increase of the shape factor. Increasing the main propulsion gas pressure can raise the spherical impact velocity with a larger shape factor, while it negligibly affects the particle impact velocity for a smaller shape factor.

The experimental observation and numerical calculation are combined to establish the relationship between the particle size, particle velocity, and spraying temperature. The selection range (deposition window) of CS process parameters for the amorphous alloy, SAM1651, was predicted by Ziemian et al. [74]. An adjusted empirical model based on Schmidt's model in [75] was used to investigate the relationship between the particle spraying conditions and deposition window. The temperature analysis was changed to account for the fact that amorphous metals do not harden nor do they behave in the same manner as crystalline materials with regard to thermal softening and impact mechanics. Through the empirical model, a relatively narrow window of successful particle adhesion was formed (Figure 17a), and proved the importance of the particle size to impact conditions and adhesion. Figure 17b showed that the experimental results were the same as the overall trend predicted by the adjusted model. At a gas temperature of 900 °C, particles with a diameter between 12 and 23 μm accounted for the largest proportion, while the proportion of particles with other sizes was much smaller. It additionally displayed evidence of the size effects and emphasizes the dependence of impact conditions and adhesion on the particle size.
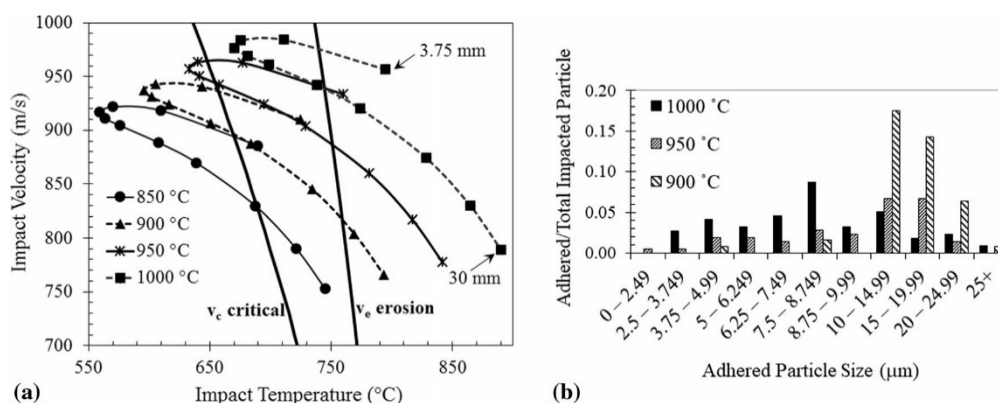

Figure 17. (**a**) Empirically derived SAM1651 amorphous alloy coating deposition window, bounded by V_c and V_e, with $T_s = 1.4\, T_g$, (**b**) the particle size ratios of different sizes were measured experimentally at 900, 950, and 1000 °C Reprint from [74] Copyright 2021 Springer.

5.2. CS Process Parameters

In the CS process, the speed and temperature of the particles are the key factors affecting the deposition and formation of the coatings, which are mainly affected by the gas temperature and pressure. In addition, the spraying distance and spray gun traverse speed also have certain effects on the microstructure and properties of the amorphous alloy coatings. In the preparation of common crystalline coating materials, the coatings can be formed only when the particle velocity reaches a critical speed. Higher gas temperatures and pressures can result in high particle velocities to improve the plastic deformation of the material, and then obtain high deposition efficiency and dense coatings. However, the deformation of amorphous particles mainly depends on the viscoplastic characteristics of the amorphous alloy in a certain temperature range. When the Re of the particles reaches a critical value, the deformation uniformity of the amorphous alloy particles can be promoted, and then the dense coatings are formed.

(1)   Gas type and temperature

Nitrogen (N$_2$), helium (He), argon (Ar), mixture gas, and compressed air are involved in CS. In the data (Table 3) collected by Prisco [76] and calculated using Sutherland's formula:

$$\mu_g = \mu_{ref} \frac{T_{ref} + C}{T + C} \left(\frac{T}{T_{ref}} \right)^{\frac{3}{2}} \tag{2}$$

where T_{ref} is a reference temperature, μ_{ref} is the viscosity at the reference temperature, T is the gas temperature, μ_g is the gas viscosity and C is the Sutherland temperature. It is shown that helium (He) has a greater viscosity, a smaller molecular weight, and a greater dynamic output than nitrogen (N$_2$), resulting in a large driving force on the particles. Using helium (He) as the working gas can greatly increase the impact velocity of particles. However, the use of helium (He) is too costly, therefore CS generally uses nitrogen (He) or compressed air as the working gas [77]. For amorphous alloys, due to its high hardness and difficulty in deformation at low temperatures, in order to obtain higher particle speeds when the pressure of cold spray equipment is low, He is often selected as the acceleration gas to prepare dense amorphous alloy coatings.

Table 3. Sutherland's reference values for some gases commonly used in CS [76].

Gas Type	C (K)	T_{ref} (K)	μ_{ref} (μ·Pa·s)	Molecular Weight
Air	120	291.15	18.27	28.96 (mean)
Nitrogen	111	300.55	17.81	28.01
Helium	99	273	19	4.00
Argon	135	300	22.9	39.94

In the combination of amorphous alloy particles, the gas temperature plays an important role. The acceleration of particles is controlled by the gas expansion into supersonic flow and heating of particles. The effect of increasing the temperature of the material above T_g will cause thermal softening and the amorphous material will exhibit homogeneous deformation. In general, in order to improve the overall deformation ability of CS amorphous alloy particles, preheating the particles to a temperature higher than the glass transition temperature can improve the deposition efficiency and overall performance of the amorphous alloy coatings.

(2)   Gas pressure

One of the most important process parameters of CS technology is the gas pressure. When the air pressure is higher, it will drive the powder to produce at a higher speed and obtain greater kinetic energy, and then undergo severe plastic deformation to form the coatings. Deposition efficiency will also increase.

Henao et al. [37] studied the influence of CS process conditions on the microstructure of Fe-based amorphous alloy coatings. Figure 18a,b showed the cross-sectional structure of the coating sprayed at different gas pressures (4 and 5 MPa) at a gas temperature of 900 °C. Generally, when the spraying conditions were fixed at 4 MPa, the thickness of the coating can reach 800 μm. In Figure 18a of the optimal spraying conditions, a dense structure with a porosity of less than 0.5% can be seen, indicating that particles deformed homogeneously upon impact. The air pressure determined the formation of the coating in this work, and also showed a low correlation between porosity, deposition efficiency, and thickness on the gas pressure. The results of efficiency, porosity, and thickness suggested that the particles were rejected from the surface upon impact at a higher gas pressure. This effect may be due to the higher impact velocity and the reduced residence time of the particles in the jet, thus changing the critical impact velocity and deformation conditions. Therefore, adjusting the appropriate pressure promotes the deformation uniformity of the amorphous alloy

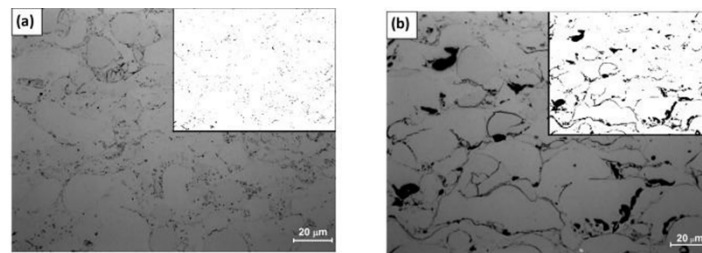particles, which is beneficial to the improvement of the deposition efficiency and density of the coatings.

Figure 18. Cross-sectional structure of the as-sprayed coatings under different gas pressures (**a**) 4 and (**b**) 5 MPa. Reprinted with permission from [37] Copyright 2021 Elsevier.

5.3. Substrate Material

The properties of the substrate material have a great influence on the deposition of CS coatings. For crystalline materials, different substrate hardness results in different strain rates upon impact. Softer substrates cause less deformation of the particles, and the particles easily penetrate the surface of the soft substrate. In contrast, harder substrates promote the flattening of particles and changes in the microstructure, such as recrystallization [78,79]. Henao et al. [80] reported that the substrate material also has an important effect on the characteristics of the amorphous alloy particle deformation, in terms of the bonding behavior and microstructure evolution. The hard substrate can improve the compactness of the metallic glass coating. It is also worth mentioning that a very hard matrix material with a large elastic limit will cause the rebound energy of the deformed particles to be high enough to rebound after impact. The thermal properties of the substrate material will affect the heat dissipation rate of the metallic glass particles during the impact. The high thermal diffusivity causes the rapid cooling of the surface, therefore the temperature of the metallic glass particles is lower than their glass transition point, resulting in inhomogeneous deformation.

5.4. Heat Treatment Process

Amorphous alloys are highly disordered and an unstable atom structure, and can change to a stable state with low energy during heating [81–83]. Therefore, the heat treatment process has a certain effect on the microstructure and characteristics of amorphous alloy coatings.

Pitchuka et al. [84] studied the dry sliding wear behavior of cold sprayed Al-based amorphous coatings at the as-sprayed and heat treatment ($300 < T_g$ 320 °C, 1 h) conditions, and explained the coating wear mechanism. The wear volume loss was 0.22 and 0.37 mm^3 for heat-treated and as-sprayed coatings, respectively. The wear volume loss was 68% higher in the as-sprayed condition. The weight loss of the sprayed coating (7.6 mg) was nearly an order of magnitude higher than that of the heat-treated sprayed coating (0.8 mg). The difference between the volume loss and mass loss was due to the combination of densification, crystallization, and improved inter-splat bonding in heat-treated coatings. The dominant wear mechanism in the as-sprayed coatings was the oxidative microabrasion and delamination of the oxide layer and splats. After the heat treatment, the dominant wear became severe plastic deformation and delamination of the deformed layer.

Choi et al. [85] investigated the crystallinity effect on the tribological behavior, by applying the heat treatment to CS $Ni_{59}Ti1_6Zr_{20}Si_2Sn_3$ amorphous coatings. Crystallization made the amorphous alloy coatings harder but it increased both the scratch friction coefficient and the worn-out cross-sectional area. From examination of the scratched wear track, a transition from ductile deformation to brittle deformation in the scratch groove was observed with an increase in the crystallinity. Babu et al. [86] studied the room temperature creep behavior of nano-indentation of CS Al-based amorphous coatings and heat treated coatings (300 °C). After the heat treatment, the stress index of the coatings was high, and

the creep resistance of the Al-based amorphous alloy coatings can be improved by the heat treatment process. The stress exponent value varies from 5.6 to 2.3 in as-sprayed coatings and 7.2 to 4.8 in heat treated coatings at a peak load of 1000–4000 mN and 240 s hold time. The higher stress exponent value indicated that heat treated coatings have more resistance to creep deformation than as-sprayed coatings. A relaxed, partially crystallized structure with less porosity, and stronger inter-splat boundaries restricted the deformation in heat treated coatings as compared to the greater free volume generation in as-sprayed coatings. The influence of the post heat treatment on the microstructure and tensile properties of the cold sprayed Zr-based metallic glass/Cu composite was studied by Kang et al. [45]. A significant increase in ductility was obtained, and the elongation reaches 26.1% after heat treating at 300 °C for 1 h.

Therefore, the heat treatment process is a very important parameter in CS. The wear resistance, creep resistance, and some mechanical properties of the coating can be improved by the heat treatment process to change the combination of densification, crystallization, and improved inter-splat bonding.

6. Summary and Outlook

Amorphous alloy coatings have shown excellent corrosion and wear resistance, which has broadened the application in the field of surface protection. Compared with high-temperature preparation processes such as thermal spraying and laser cladding, the CS technology is characterized by a low-temperature and solid deposition, which can effectively avoid thermal effects such as oxidation and crystallization, and has great potential in the preparation of high-performance amorphous alloy coatings with a complete amorphous structure.

Compared with the deposition of crystalline materials during the CS process, the particle temperature plays a critical role in influencing the deformation characteristic of amorphous alloys. The deposition mechanism of CS amorphous coatings needs to be systematically studied. In addition, the relating predication model of the deposition window should be urgently built up to better understand the process and instruct the engineering applications.

Author Contributions: Methodology, Q.W., P.H., S.Y., W.-J.N., L.Z., X.L., X.M, and. Y.H.; software, Q.W., P.H., S.Y., and W.-J.N.; validation, X.X., Y.Y. and Z.Z.; investigation, Q.W., P.H., S.Y., W.-J.N., and L.Z.; resources, Q.W.; writing—original draft preparation, Q.W., P.H., S.Y., W.-J.N., L.Z., X.L., X.M., and Y.H.; writing—review and editing, Q.W., P.H., S.Y., W.-J.N., L.Z., and X.L.; supervision, Q.W.; project administration, Q.W.; funding acquisition, Q.W. All authors have read and agreed to the published version of the manuscript.

Institutional Review Board Statement: Not applicable.

Informed Consent Statement: Not applicable.

Data Availability Statement: Not applicable.

References

1. Wang, W.H.; Dong, C.; Shek, C.H. Bulk metallic glasses. *Mater. Sci. Eng. R Rep.* **2004**, *44*, 45–89. [CrossRef]
2. Sheng, H.W.; Luo, W.K.; Alamgir, F.M.; Bai, J.M.; Ma, E. Atomic packing and short-to-medium-range order in metallic glasses. *Nature* **2006**, *439*, 419–425. [CrossRef]
3. Nie, D.; Panfilova, E.; Samusenkov, V.; Mikhaylov, A. E-learning financing models in russia for sustainable development. *Sustainability* **2020**, *12*, 4412. [CrossRef]
4. Yumashev, A.; Ślusarczyk, B.; Kondrashev, S.; Mikhaylov, A. Global indicators of sustainable development: Evaluation of the influence of the human development index on consumption and quality of energy. *Energies* **2020**, *13*, 2768. [CrossRef]
5. Johnson, W.L. Bulk amorphous metal—An emerging engineering material. *JOM* **2002**, *54*, 40–43. [CrossRef]

6. Liu, Y.H.; Wang, G.; Wang, R.J.; Zhao, D.Q.; Pan, M.X.; Wang, W.H. Super plastic bulk metallic glasses at room temperature. *Science* **2007**, *315*, 1385–1388. [CrossRef]

7. Kruzic, J.J. Bulk metallic glasses as structural materials: A review. *Adv. Eng. Mater.* **2016**, *18*, 1308–1331. [CrossRef]

8. Greer, A.L.; Ma, E. Bulk metallic glasses: At the cutting edge of metals research. *MRS Bull.* **2011**, *32*, 611–619. [CrossRef]

9. Inoue, A.; Takeuchi, A. Recent development and application products of bulk glassy alloys. *Acta Mater.* **2011**, *59*, 2243–2267. [CrossRef]

10. Miracle, D.B. A structural model for metallic glasses. *Microsc. Microanal.* **2004**, *10*, 786–787. [CrossRef]

11. Greer, A.L.; Cheng, Y.Q.; Ma, E. Shear bands in metallic glasses. *Mater. Sci. Eng. R Rep.* **2013**, *74*, 71–132. [CrossRef]

12. Das, J.; Tang, M.B.; Kim, K.B.; Theissmann, R.; Baier, F.; Wang, W.H.; Eckert, J. "Work-hardenable" ductile bulk metallic glass. *Phys. Rev. Lett* **2005**, *94*, 205501. [CrossRef] [PubMed]

13. Greer, J.R.; De Hosson, J.T.M. Plasticity in small-sized metallic systems: Intrinsic versus extrinsic size effect. *Prog. Mater. Sci.* **2011**, *56*, 654–724. [CrossRef]

14. Yoon, S.; Lee, C.; Choi, H. Evaluation of the effects of the crystallinity of kinetically sprayed Ni–Ti–Zr–Si–Sn bulk metallic glass on the scratch response. *Mater. Sci. Eng. A* **2007**, *449–451*, 285–289. [CrossRef]

15. Joshi, S.S.; Katakam, S.; Arora, H.S.; Mukherjee, S.; Dahotre, N.B. Amorphous coatings and surfaces on structural materials. *Crit. Rev. Solid State Mater. Sci.* **2015**, *41*, 1–46. [CrossRef]

16. Abrosimova, G.E. Evolution of the structure of amorphous alloys. *Phys. Uspekhi* **2011**, *54*, 1227–1242. [CrossRef]

17. Sienicki, J.; Zórawski, W.; Dworak, A.; Koruba, P.; Jurewicz, P.; Reiner, J. Cold spraying and laser cladding as an alternative to electroplating processes. *Aircr. Eng. Aerosp. Technol.* **2019**, *91*, 205–215. [CrossRef]

18. Gu, D.D.; Meiners, W.; Wissenbach, K.; Poprawe, R. Laser additive manufacturing of metallic components: Materials, processes and mechanisms. *Int. Mater. Rev.* **2013**, *57*, 133–164. [CrossRef]

19. Vardelle, A.; Moreau, C.; Themelis, N.J.; Chazelas, C. A perspective on plasma spray technology. *Plasma Chem. Plasma Process.* **2014**, *35*, 491–509. [CrossRef]

20. Fu, W.; Chen, Q.-Y.; Yang, C.; Yi, D.-L.; Yao, H.-L.; Wang, H.-T.; Ji, G.-C.; Wang, F. Microstructure and properties of high velocity oxygen fuel sprayed (WC–Co)–Ni coatings. *Ceram. Int.* **2020**, *46*, 14940–14948. [CrossRef]

21. Ding, P.; Liu, X.-J.; Liu, J.-J.; Li, J.-B.; Li, H.-Q.; Zhao, H.-Y.; Duan, J.-Y.; Jiao, Y.-Z. Study on the properties of FeCrNi/CBN composite coating with high velocity arc spraying. *Arab. J. Chem.* **2018**, *11*, 935–941. [CrossRef]

22. Cheng, J.B.; Liang, X.B.; Chen, Y.X.; Wang, Z.H.; Xu, B.S. High-temperature erosion resistance of FeBSiNb amorphous coatings deposited by arc spraying for boiler applications. *J. Therm. Spray Technol.* **2012**, *22*, 820–827. [CrossRef]

23. Ang, A.S.M.; Sanpo, N.; Sesso, M.L.; Kim, S.Y.; Berndt, C.C. Thermal spray maps: Material genomics of processing technologies. *J. Therm. Spray Technol.* **2013**, *22*, 1170–1183. [CrossRef]

24. Guo, S.F.; Pan, F.S.; Zhang, H.J.; Zhang, D.F.; Wang, J.F.; Miao, J.; Su, C.; Zhang, C. Fe-based amorphous coating for corrosion protection of magnesium alloy. *Mater. Des.* **2016**, *108*, 624–631. [CrossRef]

25. Kim, D.H.; Kim, W.T.; Park, E.S.; Mattern, N.; Eckert, J. Phase separation in metallic glasses. *Prog. Mater. Sci.* **2013**, *58*, 1103–1172. [CrossRef]

26. Guo, W.; Wu, Y.; Zhang, J.; Hong, S.; Li, G.; Ying, G.; Guo, J.; Qin, Y. Fabrication and characterization of thermal-sprayed Fe-based amorphous/nanocrystalline composite coatings: An overview. *J. Therm. Spray Technol.* **2014**, *23*, 1157–1180. [CrossRef]

27. Alkhimov, A.P.; Klinkov, S.V.; Kosarev, V.F.; Papyrin, A.N. Gas-dynamic spraying study of a plane supersonic two-phase jet. *J. Appl. Mech. Tech. Phys.* **1997**, *38*, 324–330. [CrossRef]

28. Winnicki, M.; Małachowska, A.; Dudzik, G.; Rutkowska-Gorczyca, M.; Marciniak, M.; Abramski, K.; Ambroziak, A.; Pawłowski, L. Numerical and experimental analysis of copper particles velocity in low-pressure cold spraying process. *Surf. Coat. Technol.* **2015**, *268*, 230–240. [CrossRef]

29. Raoelison, R.N.; Xie, Y.; Sapanathan, T.; Planche, M.P.; Kromer, R.; Costil, S.; Langlade, C. Cold gas dynamic spray technology: A comprehensive review of processing conditions for various technological developments till to date. *Addit. Manuf.* **2018**, *19*, 134–159. [CrossRef]

30. Assadi, H.; Schmidt, T.; Richter, H.; Kliemann, J.O.; Binder, K.; Gärtner, F.; Klassen, T.; Kreye, H. On parameter selection in cold spraying. *J. Therm. Spray Technol.* **2011**, *20*, 1161–1176. [CrossRef]

31. Assadi, H.; Kreye, H.; Gärtner, F.; Klassen, T. Cold spraying–A materials perspective. *Acta Mater.* **2016**, *116*, 382–407. [CrossRef]

32. Pattison, J.; Celotto, S.; Morgan, R.; Bray, M.; O'Neill, W. Cold gas dynamic manufacturing: A non-thermal approach to freeform fabrication. *Int. J. Mach. Tools Manuf.* **2007**, *47*, 627–634. [CrossRef]

33. Moridi, A.; Hassani-Gangaraj, S.M.; Guagliano, M.; Dao, M. Cold spray coating: Review of material systems and future perspectives. *Surf. Eng.* **2014**, *30*, 369–395. [CrossRef]

34. Wang, Q.; Zhang, M.X. Review on recent research and development of cold spray technologies. *Key Eng. Mater.* **2012**, *533*, 1–52. [CrossRef]

35. List, A.; Gärtner, F.; Schmidt, T.; Klassen, T. Impact conditions for cold spraying of hard metallic glasses. *J. Therm. Spray Technol.* **2012**, *21*, 531–540. [CrossRef]

36. Concustell, A.; Henao, J.; Dosta, S.; Cinca, N.; Cano, I.G.; Guilemany, J.M. On the formation of metallic glass coatings by means of Cold Gas Spray technology. *J. Alloy. Compd.* **2015**, *651*, 764–772. [CrossRef]

37. Henao, J.; Concustell, A.; Cano, I.G.; Cinca, N.; Dosta, S.; Guilemany, J.M. Influence of cold gas spray process conditions on the microstructure of Fe-based amorphous coatings. *J. Alloy. Compd.* **2015**, *622*, 995–999. [CrossRef]

38. Ajdelsztajn, L.; Lavernia, E.J.; Jodoin, B.; Richer, P.; Sansoucy, E. Cold gas dynamic spraying of iron-base amorphous alloy. *J. Therm. Spray Technol.* **2006**, *15*, 495–500. [CrossRef]

39. Yoon, S.; Kim, J.; Bae, G.; Kim, B.; Lee, C. Formation of coating and tribological behavior of kinetic sprayed Fe-based bulk metallic glass. *J. Alloy. Compd.* **2011**, *509*, 347–353. [CrossRef]

40. Henao, J.; Concustell, A.; Cano, I.G.; Dosta, S.; Cinca, N.; Guilemany, J.M.; Suhonen, T. Novel Al-based metallic glass coatings by Cold Gas Spray. *Mater. Des.* **2016**, *94*, 253–261. [CrossRef]

41. Choi, H.; Yoon, S.; Kim, G.; Jo, H.; Lee, C. Phase evolutions of bulk amorphous NiTiZrSiSn feedstock during thermal and kinetic spraying processes. *Scr. Mater.* **2005**, *53*, 125–130. [CrossRef]

42. Yoon, S.; Lee, C.; Choi, H.; Jo, H. Kinetic spraying deposition behavior of bulk amorphous NiTiZrSiSn feedstock. *Mater. Sci. Eng. A* **2006**, *415*, 45–52. [CrossRef]

43. List, A.; Gärtner, F.; Mori, T.; Schulze, M.; Assadi, H.; Kuroda, S.; Klassen, T. Cold spraying of amorphous Cu50Zr50 alloys. *J. Therm. Spray Technol.* **2014**, *24*, 108–118. [CrossRef]

44. Yoon, S.; Bae, G.; Xiong, Y.; Kumar, S.; Kang, K.; Kim, J.-J.; Lee, C. Strain-enhanced nanocrystallization of a CuNiTiZr bulk metallic glass coating by a kinetic spraying process. *Acta Mater.* **2009**, *57*, 6191–6199. [CrossRef]

45. Kang, N.; Coddet, P.; Liao, H.; Coddet, C. The effect of heat treatment on microstructure and tensile properties of cold spray Zr base metal glass/Cu composite. *Surf. Coat. Technol.* **2015**, *280*, 64–71. [CrossRef]

46. Liu, L.; Zhang, C. Fe-based amorphous coatings: Structures and properties. *Thin Solid Film.* **2014**, *561*, 70–86. [CrossRef]

47. Suryanarayana, C.; Inoue, A. Iron-based bulk metallic glasses. *Int. Mater. Rev.* **2013**, *58*, 131–166. [CrossRef]

48. Duarte, M.J.; Kostka, A.; Jimenez, J.A.; Choi, P.; Klemm, J.; Crespo, D.; Raabe, D.; Renner, F.U. Crystallization, phase evolution and corrosion of Fe-based metallic glasses: An atomic-scale structural and chemical characterization study. *Acta Mater.* **2014**, *71*, 20–30. [CrossRef]

49. Choi, S.J.; Lee, H.S.; Jang, J.W.; Yi, S. Corrosion behavior in a 3.5 wt.% NaCl solution of amorphous coatings prepared through plasma-spray and cold-spray coating processes. *Met. Mater. Int.* **2014**, *20*, 1053–1057. [CrossRef]

50. Shen, Y.; Perepezko, J.H. Al-based amorphous alloys: Glass-forming ability, crystallization behavior and effects of minor alloying additions. *J. Alloy. Compd.* **2017**, *707*, 3–11. [CrossRef]

51. Zhang, S.D.; Wang, Z.M.; Chang, X.C.; Hou, W.L.; Wang, J.Q. Identifying the role of nanoscale heterogeneities in pitting behaviour of Al-based metallic glass. *Corros. Sci.* **2011**, *53*, 3007–3015. [CrossRef]

52. Jeong, J.; Lee, S.; Jeon, J.-B.; Kim, S. Excessively high vapor pressure of Al-based amorphous alloys. *Metals* **2015**, *5*, 1878–1886. [CrossRef]

53. Lahiri, D.; Gill, P.K.; Scudino, S.; Zhang, C.; Singh, V.; Karthikeyan, J.; Munroe, N.; Seal, S.; Agarwal, A. Cold sprayed aluminum based glassy coating: Synthesis, wear and corrosion properties. *Surf. Coat. Technol.* **2013**, *232*, 33–40. [CrossRef]

54. Shi, H.; Liu, M.; Cong, L.; Wang, L. A study on preparation and mechanism of Ni based ternary alloy. *Mater. Express* **2019**, *9*, 681–685. [CrossRef]

55. Wang, A.P.; Zhang, T.; Wang, J.Q. Ni-based fully amorphous metallic coating with high corrosion resistance. *Philos. Mag. Lett.* **2006**, *86*, 5–11. [CrossRef]

56. Rajaei, V.; Rashtchi, H.; Raeissi, K.; Shamanian, M. The study of Ni-based nano-crystalline and amorphous alloy coatings on AISI 304 stainless steel for PEM fuel cell bipolar plate application. *Int. J. Hydrog. Energy* **2017**, *42*, 14264–14278. [CrossRef]

57. Yoon, S.; Kim, H.J.; Lee, C. Deposition behavior of bulk amorphous NiTiZrSiSn according to the kinetic and thermal energy levels in the kinetic spraying process. *Surf. Coat. Technol.* **2006**, *200*, 6022–6029. [CrossRef]

58. Wang, A.P.; Chang, X.C.; Hou, W.L.; Wang, J.Q. Preparation and corrosion behaviour of amorphous Ni-based alloy coatings. *Mater. Sci. Eng. A* **2007**, *449–451*, 277–280. [CrossRef]

59. Kim, K.H.; Lee, S.W.; Ahn, J.P.; Fleury, E.; Kim, Y.C.; Lee, J.C. A Cu-based amorphous alloy with a simultaneous improvement in its glass forming ability and plasticity. *Met. Mater. Int.* **2007**, *13*, 21–24. [CrossRef]

60. Kim, J.; Kang, K.; Yoon, S.; Lee, C. Enhancement of metallic glass properties of Cu-based BMG coating by shroud plasma spraying. *Surf. Coat. Technol.* **2011**, *205*, 3020–3026. [CrossRef]

61. Wu, J.; Peng, Z. Effects of microadditions on glass transition and hardness of Cu-based bulk metallic glasses. *Appl. Phys. A* **2018**, *124*, 632. [CrossRef]

62. Lee, K.A.; Jung, D.J.; Park, D.Y.; Kang, W.G.; Lee, J.K.; Kim, H.J. Study on the fabrication and physical properties of cold-sprayed, Cu-based amorphous coating. *J. Phys. Conf. Ser.* **2009**, *144*, 012113. [CrossRef]

63. El-Eskandrany, M.S.; Al-Azmi, A. Potential applications of cold sprayed Cu50Ti20Ni30 metallic glassy alloy powders for antibacterial protective coating in medical and food sectors. *J. Mech. Behav. Biomed. Mater.* **2016**, *56*, 183–194. [CrossRef]

64. Ma, Z.-C.; Ma, X.-X.; Zhao, H.-W.; Zhang, F.; Zhou, L.-M.; Ren, L.-Q. Novel crystallization behaviors of Zr-based metallic glass under thermo-mechanical coupled fatigue loading condition. *Acta Metall. Sin. (Engl. Lett.)* **2019**, *32*, 797–802. [CrossRef]

65. Sugita, K.; Matsumoto, M.; Mizuno, M.; Araki, H.; Shirai, Y. Electron irradiation damage and the recovery in a Zr-based bulk amorphous alloy Zr55Cu30Al10Ni5. *J. Phys. Conf. Ser.* **2008**, *106*, 012024. [CrossRef]

66. Grujicic, M.; Saylor, J.R.; Beasley, D.E.; DeRosset, W.S.; Helfritch, D. Computational analysis of the interfacial bonding between feed-powder particles and the substrate in the cold-gas dynamic-spray process. *Appl. Surf. Sci.* **2003**, *219*, 211–227. [CrossRef]

67. Assadi, H.; Gärtner, F.; Stoltenhoff, T.; Kreye, H. Bonding mechanism in cold gas spraying. *Acta Mater.* **2003**, *51*, 4379–4394. [CrossRef]

68. Yoon, S.; Lee, C.; Choi, H.; Kim, H.; Bae, J. Impacting behavior of bulk metallic glass powder at an abnormally high strain rate during kinetic spraying. *Mater. Sci. Eng. A* **2007**, *449–451*, 911–915. [CrossRef]

69. Hufnagel, T.C.; Schuh, C.A.; Falk, M.L. Deformation of metallic glasses: Recent developments in theory, simulations, and experiments. *Acta Mater.* **2016**, *109*, 375–393. [CrossRef]

70. Henao, J.; Concustell, A.; Dosta, S.; Bolelli, G.; Cano, I.G.; Lusvarghi, L.; Guilemany, J.M. Deposition mechanisms of metallic glass particles by Cold Gas Spraying. *Acta Mater.* **2017**, *125*, 327–339. [CrossRef]

71. Schmidt, T.; Gaertner, F.; Kreye, H. New developments in cold spray based on higher gas and particle temperatures. *J. Therm. Spray Technol.* **2006**, *15*, 488–494. [CrossRef]

72. Song, J.; Liu, J.; Chen, Q.; Li, K. Effect of the shape factor on the cold-spraying dynamic characteristics of sprayed particles. *J. Therm. Spray Technol.* **2017**, *26*, 1851–1858. [CrossRef]

73. Gu, S.; Kamnis, S. Numerical modelling of in-flight particle dynamics of non-spherical powder. *Surf. Coat. Technol.* **2009**, *203*, 3485–3490. [CrossRef]

74. Ziemian, C.W.; Wright, W.J.; Cipoletti, D.E. Influence of impact conditions on feedstock deposition behavior of cold-sprayed Fe-based metallic glass. *J. Therm. Spray Technol.* **2018**, *27*, 843–856. [CrossRef]

75. Schmidt, T.; Gärtner, F.; Assadi, H.; Kreye, H. Development of a generalized parameter window for cold spray deposition. *Acta Mater.* **2006**, *54*, 729–742. [CrossRef]

76. Prisco, U. Size-dependent distributions of particle velocity and temperature at impact in the cold-gas dynamic-spray process. *J. Mater. Process. Technol.* **2015**, *216*, 302–314. [CrossRef]

77. Schmidt, T.; Assadi, H.; Gärtner, F.; Richter, H.; Stoltenhoff, T.; Kreye, H.; Klassen, T. From particle acceleration to impact and bonding in cold spraying. *J. Therm. Spray Technol.* **2009**, *18*, 794–808. [CrossRef]

78. Bae, G.; Xiong, Y.; Kumar, S.; Kang, K.; Lee, C. General aspects of interface bonding in kinetic sprayed coatings. *Acta Mater.* **2008**, *56*, 4858–4868. [CrossRef]

79. Yin, S.; Wang, X.-F.; Li, W.-Y.; Guo, X.-P. Examination on substrate preheating process in cold gas dynamic spraying. *J. Therm. Spray Technol.* **2011**, *20*, 852–859. [CrossRef]

80. Henao, J.; Concustell, A.; Dosta, S.; Cinca, N.; Cano, I.G.; Guilemany, J.M. Influence of the substrate on the formation of metallic glass coatings by cold gas spraying. *J. Therm. Spray Technol.* **2016**, *25*, 992–1008. [CrossRef]

81. Ievlev, V.M.; Kannykin, S.V.; Il'inova, T.N.; Vavilova, V.V.; Kushchev, S.B.; Serikov, D.V.; Baikin, A.S. Heat treatment- and lamp processing-induced structural transformations of an amorphous $Fe_{77}B_7Nb_{2.1}Si1_3Cu_{0.9}$ alloy and nonmonotonic behavior of its mechanical properties. *Inorg. Mater.* **2019**, *55*, 659–668. [CrossRef]

82. Kozlov, I.V.; Elmanov, G.N.; Prikhodko, K.E.; Kutuzov, L.V.; Tarasov, B.A.; Mikhalchik, V.V.; Svetogorov, R.D.; Mashera, V.S.; Gorelikov, E.S.; Gudoshnikov, S.A. The evolution of structure and magnetoimpedance characteristics of amorphous $Co_{69}Fe_4Cr_4Si_{12}B_{11}$ microwires under heat treatment. *J. Magn. Magn. Mater.* **2020**, *493*, 493. [CrossRef]

83. Zheng, Z.B.; Zheng, Y.G.; Sun, W.H.; Wang, J.Q. Effect of heat treatment on the structure, cavitation erosion and erosion–corrosion behavior of Fe-based amorphous coatings. *Tribol. Int.* **2015**, *90*, 393–403. [CrossRef]

84. Pitchuka, S.B.; Boesl, B.; Zhang, C.; Lahiri, D.; Nieto, A.; Sundararajan, G.; Agarwal, A. Dry sliding wear behavior of cold sprayed aluminum amorphous/nanocrystalline alloy coatings. *Surf. Coat. Technol.* **2014**, *238*, 118–125. [CrossRef]

85. Choi, H.; Jo, H.; An, K.; Yoon, S.; Lee, C. Tribological behavior of the kinetic sprayed $Ni_{59}Ti_{16}Zr_{20}Si_2Sn_3$ bulk metallic glass. *J. Alloy. Compd.* **2007**, *434–435*, 64–67. [CrossRef]

86. Babu, P.S.; Jha, R.; Guzman, M.; Sundararajan, G.; Agarwal, A. Indentation creep behavior of cold sprayed aluminum amorphous/nano-crystalline coatings. *Mater. Sci. Eng. A* **2016**, *658*, 415–421. [CrossRef]